High-Resolution Solution Structure of the Inhibitor-Free Catalytic Fragment of Human Fibroblast Collagenase Determined by Multidimensional NMR‡

Franklin J. Moy, Pranab K. Chanda,§ Scott Cosmi,§ Michael R. Pisano,§ Charlotte Urbano,§ Jim Wilhelm,§ and Robert Powers*

Department of Structural Biology and Department of Core Biotechnology, Wyeth-Ayerst Research, Pearl River, New York 10965

Received September 3, 1997; Revised Manuscript Received November 10, 1997

ABSTRACT: The high-resolution solution structure of the inhibitor-free catalytic fragment of human fibroblast collagenase (MMP-1), a protein of 18.7 kDa, which is a member of the matrix metalloproteinase family, has been determined using three-dimensional heteronuclear NMR spectroscopy. A total of 30 structures were calculated by means of hybrid distance geometry-simulated annealing using a total of 3333 experimental NMR restraints, consisting of 2409 approximate interproton distance restraints, 84 distance restraints for 42 backbone hydrogen bonds, 426 torsion angle restraints, 125 $^3J_{NH\alpha}$ restraints, 153 Cα restraints, and 136 Cβ restraints. The atomic rms distribution about the mean coordinate positions for the 30 structures for residues 7−137 and 145−163 is 0.42 ± 0.04 Å for the backbone atoms, 0.80 ± 0.04 Å for all atoms, and 0.50 ± 0.03 Å for all atoms excluding disordered side chains. The overall structure of MMP-1 is composed of a β-sheet consisting of five β-strands in a mixed parallel and anti-parallel arrangement and three α-helices. A best-fit superposition of the NMR structure of inhibitor-free MMP-1 with the 1.56 Å resolution X-ray structure by Spurlino et al. [Spurlino, J. C., Smallwood, A. M., Carlton, D. D., Banks, T. M., Vavra, K. J., Johnson, J. S., Cook, E. R., Falvo, J., and Wahl, R. C., et al. (1994) *Proteins: Struct., Funct., Genet. 19,* 98−109] complexed with a hydroxamate inhibitor yields a backbone atomic rms difference of 1.22 Å. The majority of differences between the NMR and X-ray structure occur in the vicinity of the active site for MMP-1. This includes an increase in mobility for residues 138−144 and a displacement for the Ca^{2+}-loop (residues 74−80). Distinct differences were observed for side-chain torsion angles, in particular, the χ_1 for N80 is −60° in the NMR structure compared to 180° in the X-ray. This results in the side chain of N80 occupying and partially blocking access to the active site of MMP-1.

The matrix metalloproteinase (MMP)[1] family, which includes the collagenases, stromelysins, and gelatinases, is involved in the degradation of the extracellular matrix which is associated with normal tissue remodeling processes such as pregnancy, wound healing, and angiogenesis (*2*−*4*). These enzymes are modular with both propeptide and catalytic domains being common to the entire family (*5, 6*) while requiring both zinc and calcium for catalytic activity (*7*−*9*). MMP expression and activity is highly controlled because of the degradative nature of these enzymes. The MMPs are regulated by either specific inhibitors (tissue inhibitor of metalloendoproteases, TIMP), by cleavage of the inactive proenzyme or by transcription induction or suppression (*3*). A number of biochemical stimuli including cytokines, hormones, oncogene products and tumor promoters also effect the synthesis and activation of MMPs (*2, 3*). Consequently, the MMPs have been implicated in a variety of diseases caused by uncontrolled matrix degradation, including tumor metastasis, osteo- and rheumatoid arthritis, corneal ulceration, and periodontitis (*10*) making the MMPs an attractive target for structure based drug design (*11, 12*).

The high-resolution structure of an enzyme free of either ligand or inhibitor provides an initial framework from which a structure-based drug development program is established. The rational for this approach is that future NMR refinements and analysis of enzyme−ligand complexes are determined by difference to enzyme-free NMR spectra. Additionally, valuable structural information may also be obtained from understanding any conformational change induced in the enzyme upon binding an inhibitor. Therefore, a structural program to determine the high-resolution NMR solution structure of the inhibitor-free catalytic fragment of human fibroblast collagenase was initiated. In a previous paper (*13*), we presented the near complete ^{1}H, ^{15}N, ^{13}CO, and ^{13}C assignments, solution secondary structure, and dynamics for MMP-1 which comprise the essential foundation for such a study. In this paper, we present the determination of a high-resolution solution structure of inhibitor-free MMP-1 using three-dimensional heteronuclear NMR spectroscopy. The resulting high-resolution solution structure is based on a total

‡ Atomic coordinates for the 30 final simulated annealing structures and the restrained minimized mean structure of MMP-1 have been deposited in the Brookhaven Protein Data Bank (PDB ID code 1ayk and 2ayk, respectfully).

* Corresponding author.

[1] Abbreviations: MMP, matrix metalloproteinase; NMR, nuclear magnetic resonance; 1D, one-dimensional; 2D, two-dimensional; 3D, three-dimensional; HSQC, heteronuclear single-quantum coherence spectroscopy; HMQC, heteronuclear multiple-quantum coherence spectroscopy; TPPI, time-proportional phase incrementation; NOE, nuclear Overhauser effect; NOESY, nuclear Overhauser enhanced spectroscopy.

S0006-2960(97)02181-8 CCC: $15.00
Published on Web 01/27/1998

of 3333 experimental NMR restraints with the atomic rms distribution about the mean coordinate position for residues 7−137 and 145−163 is 0.42 ± 0.04 Å for the backbone atoms and 0.80 ± 0.04 Å for all atoms.

There have been a number of X-ray and NMR structures solved for the catalytic domain of MMPs complexed with a variety of inhibitors (*1, 8, 14*−*20*) and a crystal structure of collagenase complexed to itself (*21*), but because of the proteolytic nature of these enzymes and the resulting self-cleavage and degradation, structural information of inhibitor-free MMPs has not been readily available. A comparison of the inhibitor-free NMR structure of MMP-1 with the 1.56 Å resolution X-ray structure by Spurlino et al. (*1*) indicates distinct differences between the inhibitor-free NMR structure and the X-ray structure complexed with a hydroxamate inhibitor. As expected, these differences occur primarily in the vicinity of the enzymes active site.

MATERIALS AND METHODS

NMR Sample Preparation. Uniformly (>95%) ^{15}N- and ^{15}N/^{13}C-labeled human recombinant MMP-1 was expressed in *Escherichia coli* and purified as described previously (*1, 13*) except that anion exchange was carried out on Source 30Q anion exchange resin (Pharmacia, Piscataway, NJ). Samples for NMR contained 1 mM ^{15}N- or ^{15}N/^{13}C-labeled MMP-1, pH 6.5, dissolved in a buffer containing 10 mM deuterated Tris-Base, 100 mM NaCl, 5 mM $CaCl_2$, 0.1 mM $ZnCl_2$, 2 mM NaN_3, and 10 mM deuterated DTT in either 90% H_2O/10% D_2O or 100% D_2O.

NMR Data Collection. All spectra were recorded at 35 °C on a Bruker AMX600 spectrometer using a gradient enhanced triple-resonance ^{1}H/^{13}C/^{15}N probe. For spectra recorded in H_2O, water suppression was achieved with the WATERGATE sequence and water-flip back pulses (*22, 23*). Quadrature detection in the indirectly detected dimensions were recorded with States−TPPI hypercomplex phase increment (*24*). Spectra were collected with appropriate refocusing delays to allow for 0,0 or −90,180 phase correction.

The present structure is based on the following series of spectra: HNHA (*25*), HNHB (*26*), 3D long-range ^{13}C-^{13}C correlation (*27*), coupled CT-HCACO (*28, 29*), HACAHB-COSY (*30*), 3D ^{15}N- (*31, 32*) and ^{13}C-edited NOESY (*33, 34*), and ^{15}N-edited ROESY (*35*). The ^{15}N-edited NOESY, ^{13}C-edited NOESY, and ^{15}N-edited ROESY experiments were collected with 100 ms, 120 ms, and 40 ms mixing times, respectively. The acquisition parameters for each of the experiments used in determining the solution structure of MMP-1 were as reported previously (*36*).

Spectra were processed using the NMRPipe software package (*37*) and analyzed with PIPP (*38*) on a Sun Sparc Workstation. When appropriate, data processing included a solvent filter, zero-padding data to a power of 2, linear predicting back one data point of indirectly acquired data to obtain zero phase corrections, and linear prediction of additional points for the indirectly acquired dimensions to increase resolution. Linear prediction by the means of the mirror image technique was used only for constant-time experiments (*39*). In all cases, data was processed with a skewed sine-bell apodization function and one zero-filling was used in all dimensions.

Interproton Distance Restraints. The NOEs assigned from the 3D ^{15}N- and ^{13}C-edited NOESY experiments were classified into strong, medium, weak, and very weak corresponding to interproton distance restraints of 1.8−2.7 Å (1.8−2.9 Å for NOEs involving NH protons), 1.8−3.3 Å (1.8−3.5 Å for NOEs involving NH protons), 1.8−5.0 Å, and 1.8−6.0 Å, respectively (*40, 41*). Upper distance limits for distances involving methyl protons and nonstereospecifically assigned methylene protons were corrected appropriately for center averaging (*42*), and an additional 0.5 Å was added to upper distance limits for NOEs involving methyl protons (*43, 44*). Hydrogen bond restraints were deduced on the basis of slowly exchanging NH protons which were identified by recording an HSQC spectra two days after exchanging an MMP-1 sample from H_2O to D_2O. Two distance restraints were used for each hydrogen bond (r_{NH-O} = 1.5−2.3 Å, r_{N-O} = 2.4−3.3 Å).

Torsion Angle Restraints and Stereospecific Assignments. The β-methylene stereospecific assignments and χ_1 torsion angle restraints were obtained primarily from a qualitative estimate of the magnitude of $^3J_{\alpha\beta}$ coupling constants from the HACAHB-COSY experiment (*30*) and $^3J_{N\beta}$ coupling constants from the HNHB experiment (*26*). Further support for the assignments was obtained from approximate distance restraints for intraresidue NOEs involving NH, CαH, and CβH protons (*45*).

The ϕ and ψ torsion angle restraints were obtained from $^3J_{NH\alpha}$ coupling constants measured from the relative intensity of Hα cross-peaks to the NH diagonal in the HNHA experiment (*25*), from a qualitative estimate of the magnitude of $^3J_{\alpha\beta}$ coupling constants from the HACAHB-COSY experiment (*30*) and from approximate distance restraints for intraresidue and sequential NOEs involving NH, CαH, and CβH protons by means of the conformational grid search program STEREOSEARCH (*46*), as described previously (*47*). $^1J_{C\alpha H\alpha}$ coupling constants obtained from a coupled 3D CT-HCACO spectrum were used to ascertain the presence of non-glycine residues with positive ϕ backbone torsion angles (*29*). The presence of a $^1J_{C\alpha H\alpha}$ coupling constant greater then 130 Hz allowed for a minimum ϕ restraint of −2 to −178°.

The Ile and Leu χ_2 torsion angle restraints and the stereospecific assignments for leucine methyl groups were determined from $^3J_{C\alpha C\delta}$ coupling constants obtained from the relative intensity of Cα and Cδ cross peaks in a 3D long-range ^{13}C-^{13}C NMR correlation spectrum (*48*), in conjunction with the relative intensities of intraresidue NOEs (*49*). Stereospecific assignments for valine methyl groups were determined based on the relative intensity of intraresidue NH-CγH and CαH-CγH NOEs as described by Zuiderweg et al. (*50*). The minimum ranges employed for the ϕ, ψ, and χ torsion angle restraints were ±30°, ±50°, and ±20°, respectively (*47*).

Structure Calculations. The structures were calculated using the hybrid distance geometry-dynamical simulated annealing method of Nilges et al. (*51*) with minor modifications (*52*) using the program XPLOR (*53*), adapted to incorporate pseudopotentials for $^3J_{NH\alpha}$ coupling constants (*54*), secondary ^{13}Cα/^{13}Cβ chemical shift restraints (*55*) and a conformational database potential (*56, 57*). The target function that is minimized during restrained minimization and simulated annealing comprises only quadratic harmonic

Table 1: Structural Statistics and Atomic rms Differences[a]

A. Structural Statistics

	⟨SA⟩	$(\overline{SA})_r$	X-ray[b]
rms deviations from experimental distance restraints (Å)[c]			
all (2493)	0.011 ± 0.002	0.014	0.121
interresidue sequential ($\|i-j\| = 1$) (708)	0.009 ± 0.003	0.011	0.116
interresidue short range ($1 < \|i-j\| \geq 5$) (490)	0.012 ± 0.003	0.013	0.133
interresidue long-range ($\|i-j\| > 5$) (656)	0.012 ± 0.002	0.017	0.137
intraresidue (555)	0.005 ± 0.006	0.000	0.083
H-bonds (84)[d]	0.029 ± 0.004	0.034	0.144
rms deviation from exptl dihedral restraints (deg) (426)[c,e]	0.118 ± 0.040	0.137	18.9
rms deviation from exptl Cα restraints (ppm) (153)	1.15 ± 0.02	1.12	1.15
rms deviation from exptl Cβ restraints (ppm) (136)	1.14 ± 0.02	1.19	1.16
rms deviation from $^3J_{NH\alpha}$ restraints (Hz) (125)	0.63 ± 0.02	0.64	1.16
F_{NOE} (kcal mol^{-1})[f]	16.2 ± 6.3	22.57	1765
F_{tor} (kcal mol^{-1})[f]	0.40 ± 0.26	0.464	8187
F_{repel} (kcal mol^{-1})[f]	49.7 ± 6.1	105.0	278
F_{L-J} (kcal mol^{-1})[g]	−668 ± 11	−617	−954
deviations from idealized covalent geometry			
bonds (Å) (2604)	0.004 ± 0	0.003	0.033
angles (deg) (4669)	0.654 ± 0.011	0.706	4.181
impropers (deg) (1434)[h]	0.399 ± 0.042	0.364	20.84
PROCHECK[i]			
overall G-Factor	0.20 ± 0.01	0.17	-0.40
% residues in most favorable region of Ramachandran plot	89.3 ± 1.1	89.9	92.4
H-bond energy	0.77 ± 0.05	0.90	0.80
number of bad contacts/100 residues	5.3 ± 1.2	4.1	0

B. Atomic rms Differences (Å)

	residues 7−137,145−163		secondary structure[k]		
	backbone atoms	all atoms	backbone atoms	all atoms	ordered side chain,[l] all atoms
⟨SA⟩ vs $\overline{SA}$	0.42 ± 0.04	0.80 ± 0.04	0.28 ± 0.04	0.64 ± 0.05	0.50 ± 0.03
⟨SA⟩ vs $(\overline{SA})_r$	0.46 ± 0.04	0.90 ± 0.05	0.31 ± 0.04	0.72 ± 0.06	0.73 ± 0.05
$(\overline{SA})_r$ vs $\overline{SA}$	0.18	0.40	0.14	0.34	0.54
$\overline{SA}$ vs X-ray	1.21	1.60	0.97	1.28	1.32
$(\overline{SA})_r$ vs X-ray	1.22	1.69	0.97	1.39	1.40
⟨SA⟩ vs X-ray	1.28 ± 0.06	1.79 ± 0.06	1.01 ± 0.05	1.45 ± 0.07	1.41 ± 0.04

[a] The notation of the structures is as follows: ⟨SA⟩ are the final 30 simulated annealing structures; $\overline{SA}$ is the mean structure obtained by averaging the coordinates of the individual SA structures best fit to each other (excluding residues 1−6, 138−144, and 164−169); and $(\overline{SA})_r$ is the restrained minimized mean structure (residues 7−163) obtained by restrained minimization of the mean structure $\overline{SA}$ (*51*). The number of terms for the various restraints is given in parentheses. [b] X-ray is the 1.56 Å resolution X-ray structure of Spurlino et al. (*1*). Tyr and Phe χ_2 dihedral angles in the X-ray structure were changed to be consistent with the NMR structure since it is not possible to differentiate between +90° or −90° in the X-ray structure. Without this correction, the calculation of F_{NOE} and F_{tor} would be artificially high for the X-ray structure. Residues 1−6 and 163−169 are not present in the X-ray structure. [c] None of the structures exhibited distance violations greater than 0.1 Å or dihedral angle violations greater than 1°. [d] For backbone NH-CO hydrogen bond there are two restraints: $r_{NH-O} = 1.5-2.3$ Å and $r_{N-O} = 2.5-3.3$ Å. All hydrogen bonds involve slowly exchanging NH protons. [e] The torsion angle restraints comprise 155 ϕ, 134 ψ, 103 χ_1 and 34 χ_2 restraints. [f] The values of the square-well NOE (F_{NOE}) and torsion angle (F_{tor}) potentials [cf. eqs 2 and 3 in Clore et al. (*41*)] are calculated with force constants of 50 kcal mol^{-1} Å^{-2} and 200 kcal mol^{-1} rad^{-2}, respectively. The value of the quartic van der Waals repulsion term (F_{rep}) [cf. eq 5 in Nilges et al. (*51*)] is calculated with a force constant of 4 kcal mol^{-1} Å^{-4} with the hard-sphere van der Waals radius set to 0.8 times the standard values used in the CHARMM empirical energy function (*67*). [g] E_{L-J} is the Lennard-Jones-van der Waals energy calculated with the CHARMM empirical energy function and is *not* included in the target function for simulated annealing or restrained minimization. [h] The improper torsion restraints serve to maintain planarity and chirality. [i] These were calculated using the PROCHECK program (Laskowski et al., 1993). [k] The residues in the regular secondary structure are 13−19 (β_1), 48−53 (β_2), 59−65 (β_3), 82−85 (β_4), 94−99 (β_5), 27−43 (α_1), 112−124 (α_2), and 150−160 (α_3). [l] The disordered side chains that were excluded are as follows: residues 1−6; residues 138−144; residues 164−169; Arg 8 from Cδ; Glu 10 from Cδ; Gln 11 from Cδ; Arg 17 beyond Cδ; Glu 19 from Cδ; Asn 20 from Cγ; Asp 24 from Cγ; Arg 27 beyond Cδ; Asp 31 from Cγ; Glu 35 from Cδ; Lys 36 from Cϵ; Gln 39 from Cδ; Asn 43 beyond Cγ; Lys 51 from Cϵ; Glu 54 from Cγ; Gln 56 from Cδ; Arg 65 beyond Cδ; Asp 70 from Cγ; Asn 71 from Cγ; Asp 75 from Cγ; Gln 86 from Cδ; Glu 99 from Cδ; Glu 101 from Cδ; Arg 102 beyond Cδ; Asn 105 beyond Cδ; Phe 107 from Cγ; Argl 108 beyond Cδ; Glu 109 from Cδ; Asn 111 from Cγ; Arg 114 beyond Cδ; Glu 119 from Cδ; Ser 123 beyond Cβ; Ile 132 from Cγ; Asp 145 from Cβ; Gln 147 from Cδ; Gln 150 from Cδ; Gln 157 from Cδ; and Arg 162 beyond Cδ.

terms for covalent geometry, $^3J_{NH\alpha}$ coupling constants and secondary $^{13}C\alpha/^{13}C\beta$ chemical shift restraints, square-well quadratic potentials for the experimental distance and torsion angle restraints, and a quartic van der Waals term for nonbonded contacts. All peptide bonds were constrained to be planar and trans. There were no hydrogen-bonding, electrostatic, or 6-12 Lennard-Jones empirical potential energy terms in the target function. The structure determination followed an iterative structure refinement procedure which has been previously described in detail (*49*, *58*, *59*). The simulated annealing protocol for MMP-1 followed a two-stage procedure. In the first stage, the simulated annealing structures were determined based on the experimental distance and dihedral restraints similar to previous structure calculations (*36*, *45*, *58*). The resulting structures were then used as initial structures for the second stage of simulated annealing calculations where, in addition to the distance and dihedral restraints, the structures were refined

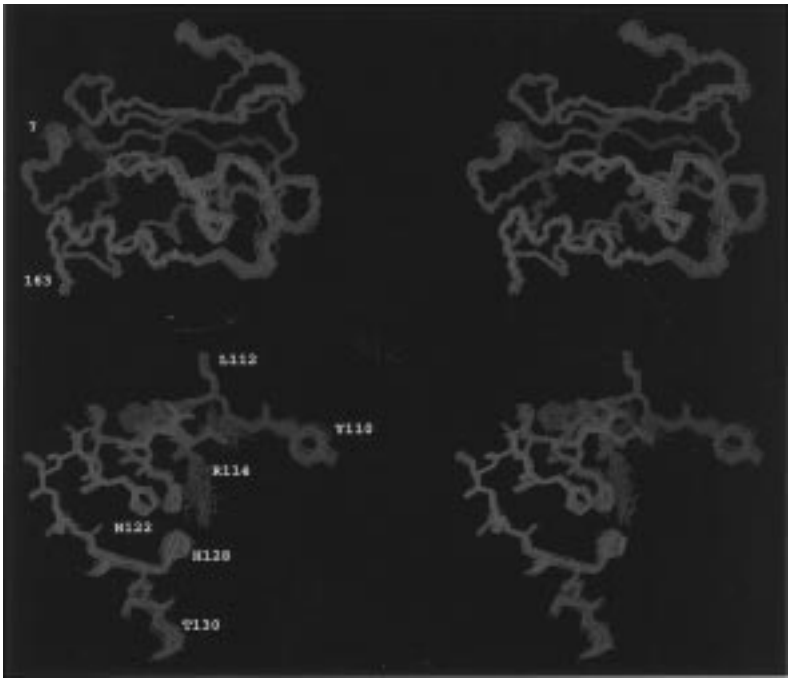

FIGURE 1: Stereoviews showing the best fit superposition of the (A) backbone (N, Cα, and C) and (B) all atoms of the 30 final simulated annealing structures. Residues 7−163 and 110−130 are shown in panels A and B, respectively.

against $^3J_{NH\alpha}$ coupling constants, secondary $^{13}C\alpha/^{13}C\beta$ chemical shift restraints and a conformational database potential.

The Zn and Ca ions were only added to the structures at the end of the iteration procedure when the resulting structures were relatively well-defined. To prevent the Zn and Ca ions from being expelled during the high-temperature simulated annealing stages of the refinement protocol a minimal number of distance restraints between the His side chain and Zn and between backbone atoms and Ca were included in the XPLOR distance restraint file based on the observed coordination in the X-ray structures (*1, 19, 21, 60*).

Tightly Bound Water. The presence of tightly bound water molecules in the MMP-1 structure were identified from the 3D ^{15}N-edited ROESY spectrum by the observation of ROEs from the water frequency (4.75 ppm) to NH protons (*35, 61*−*63*). A number of other cross-peaks were observed but could not be distinguished between an ROE to water or to a spatially close CαH or a rapidly exchanging group (e.g., the hydroxyl group of Ser or Thr). The tightly bound water molecules were identified after completion of the simulated annealing calculations and were not included in the refinement process.

RESULTS AND DISCUSSION

Structure Determination. The final 30 simulated annealing structures were calculated on the basis of 3333 experimental NMR restraints consisting of 2493 approximate interproton distance restraints, 84 distance restraints for 42 backbone hydrogen bonds, 426 torsion angle restraints comprised of 155 ϕ, 134 ψ, 103 χ_1, and 34 χ_2 torsion angle restraints, 125 $^3J_{NH\alpha}$ restraints and 153 Cα and 136 Cβ chemical shift restraints. Stereospecific assignments were obtained for 79 of the 103 residues with β-methylene protons, for the methyl groups of 6 of the 8 Val residues, and for the methyl groups of 11 of the 12 Leu residues. In addition, 6 out of the 8 Phe residues and 6 out of the 6 Tyr residues were well-defined, making it possible to assign NOE restraints to only one of the pair of CδH and CϵH protons and to assign a χ_2 torsion angle restraint. Similarly, χ_2 torsion angle restraints were assigned for the three Trp residues. A summary of the structural statistics for the final 30 simulated annealing (SA) structures of human MMP-1 is provided in Table 1, and a best fit superposition of the backbone atoms and selected side chains are shown in Figure 1. The atomic rms distribution of the 30 simulated annealing structures about the mean coordinate positions for residues 7−137 and 145−163 is 0.42 ± 0.04 Å for the backbone atoms, 0.80 ± 0.04 Å for all atoms, and 0.50 ± 0.03 Å for all atoms excluding disordered surface side chains (Table 1). The mean standard deviation for the ϕ and ψ backbone torsion angles of residues 7−137 and 145−163 are 3.1 ± 3.8° and 4.1 ± 3.9°, respectively. The atomic rms distribution about the mean coordinate positions and the angular rms deviations for the ϕ, ψ, χ_1, and χ_2 torsion angles, together with the variations in surface accessibility, are also shown in Figure 2 as a function of residue number. The high quality of the MMP-1 NMR structure is also evident by the results of PROCHECK analysis and by a calculated, large negative value for the Lennard-Jones-van der Waals energy (−668 ± 11 kcal mol^{-1}). For the PROCHECK statistics, an overall *G*-factor of 0.20 ± 0.01, a hydrogen bond energy of 0.77 ± 0.05 and only 5.3 ± 1.2 bad contacts per 100 residues are consistent with a good quality structure comparable to ∼1 Å X-ray structure.

The high quality of the MMP-1 NMR structure is also evident by the very small deviations from idealized covalent geometry, by the absence of interproton distance and torsion angle violations greater than 0.1 Å and 1°, respectively, and by the fact that most of the backbone torsion angles for non-glycine residues lie within expected regions of the Ramachandran plot (Figure 3). A total of 89.9% of the residues

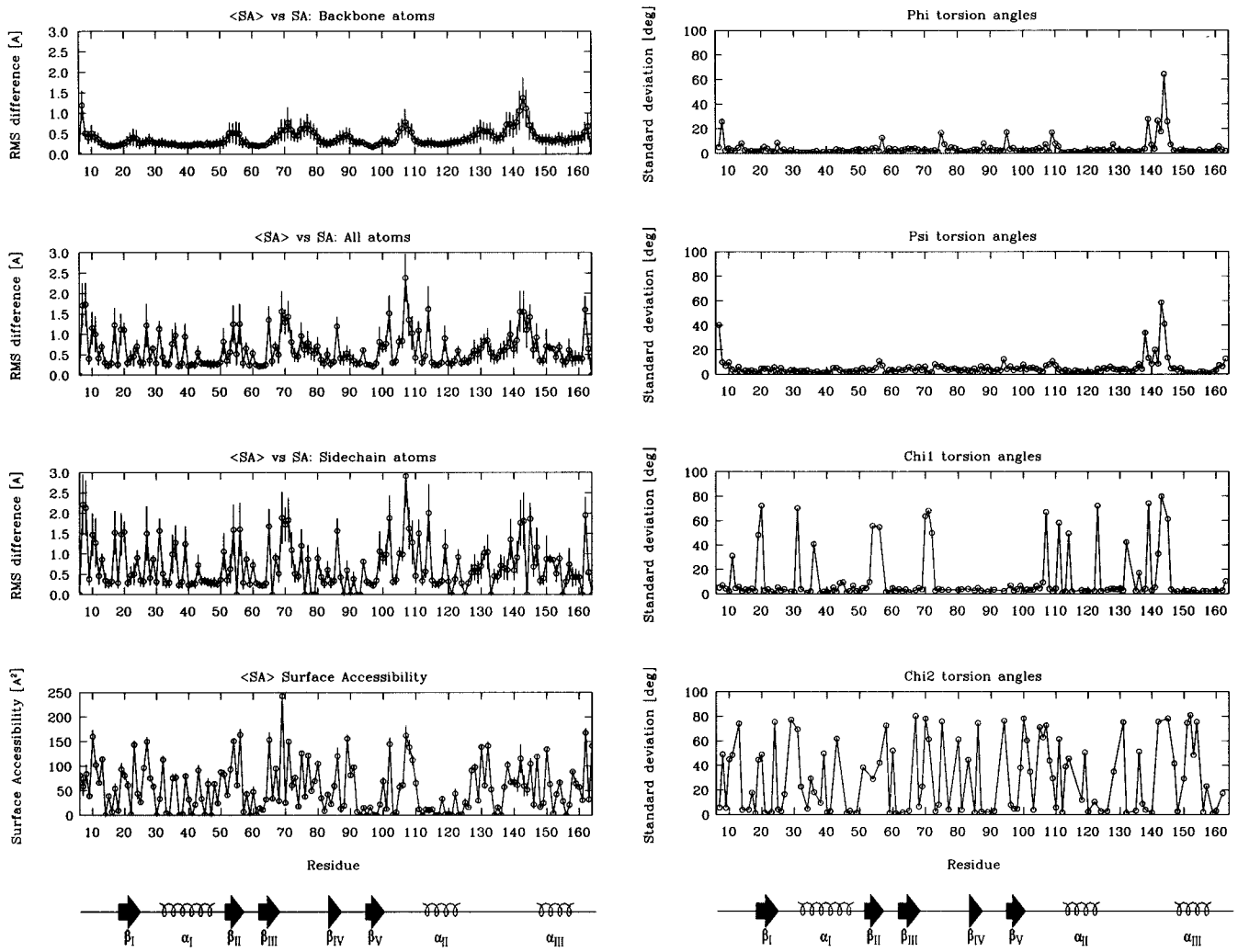

FIGURE 2: Atomic rms distribution of the 30 individual simulated annealing structures about the mean structure, for the backbone (N, Cα, C, and O) atoms, all atoms, and side-chain atoms as a function of residue number, together with the variation in surface accessibility of each residue (left). Standard deviation of the backbone ϕ and ψ and side-chain χ_1 and χ_1 torsion angles for the 30 simulated annealing structure as a function of residue number (right). The circles represent the average value at each residue, and the error bars indicate the standard deviations in these values. The bottom of the figure presents a schematic diagram of the secondary structure of MMP-1, with β-strands shown as arrows and α-helices shown as coils.

lie within the most favored region of the Ramachandran ϕ, ψ plot, 9.3% in the additionally allowed regions, and 0.8% in the generously allowed region. $^1J_{C\alpha H\alpha}$ coupling constants from the coupled CT-HCACO experiment indicated that all non-glycine residues have negative ϕ torsion angles.

Description of the Structure. A ribbon diagram of the restrained minimized average structure of MMP-1 is depicted in Figure 4. The overall structure of MMP-1 is comprised of a five-stranded mixed parallel and anti-parallel β-sheet, where strand I extends from residues 13 to 19, strand II from 48 to 52, strand III from 59 to 65, strand IV from 82 to 85, and strand V from 94 to 99; and three α-helices, where helix A corresponds to residues 27−43, helix B corresponds to residues 112−123, and helix C corresponds to residues 150−160. The active site of MMP-1 is bordered by β-strand IV, the Ca^{2+} binding loop, helix B, and a random coil region from residues P138 to Y140. The catalytic zinc is chelated by H118, H122, and H128 while the structural zinc is chelated by H68, H83, and H96. All the histidines are protonated at Nδ1 except H96, which is protonated at Nϵ2. The protonation state of H96 was inferred from its χ_1 torsion angle. The calcium ion is chelated in a loop region consisting of residues D75−G79. An interesting feature of the MMP-1 active site is an apparent kink in the backbone that occurs at L81 between the Ca^{2+} binding loop and β-strand IV. This results in the NHs of both L81 and A82 facing toward the active site of the enzyme. In previous X-ray structures of inhibited MMP-1, a significant number of hydrogen bond interactions have been observed between the inhibitor and MMP-1 in this kinked region (G79−A82) (*1*, *19*, *21*, *60*), implying that this unusual conformation probably optimizes a hydrogen-bonding network with the native collagen substrate.

Two views of a GRASP rendition of the MMP-1 active site is shown in Figure 5 where blue and red indicate positively and negatively charged surfaces, respectively. A major feature of the MMP-1 active site is the deep hydrophobic S1′ pocket with a positively charged surface at the bottom due to the capping of the pocket by R114. The catalytic zinc is to the left of the S1′ pocket creating the additional positive surface in the GRASP figure. Another feature of the MMP-1 active site is the negatively charged region toward the back of the GRASP surface corresponding to the protein backbone of residues A82 and L81. These

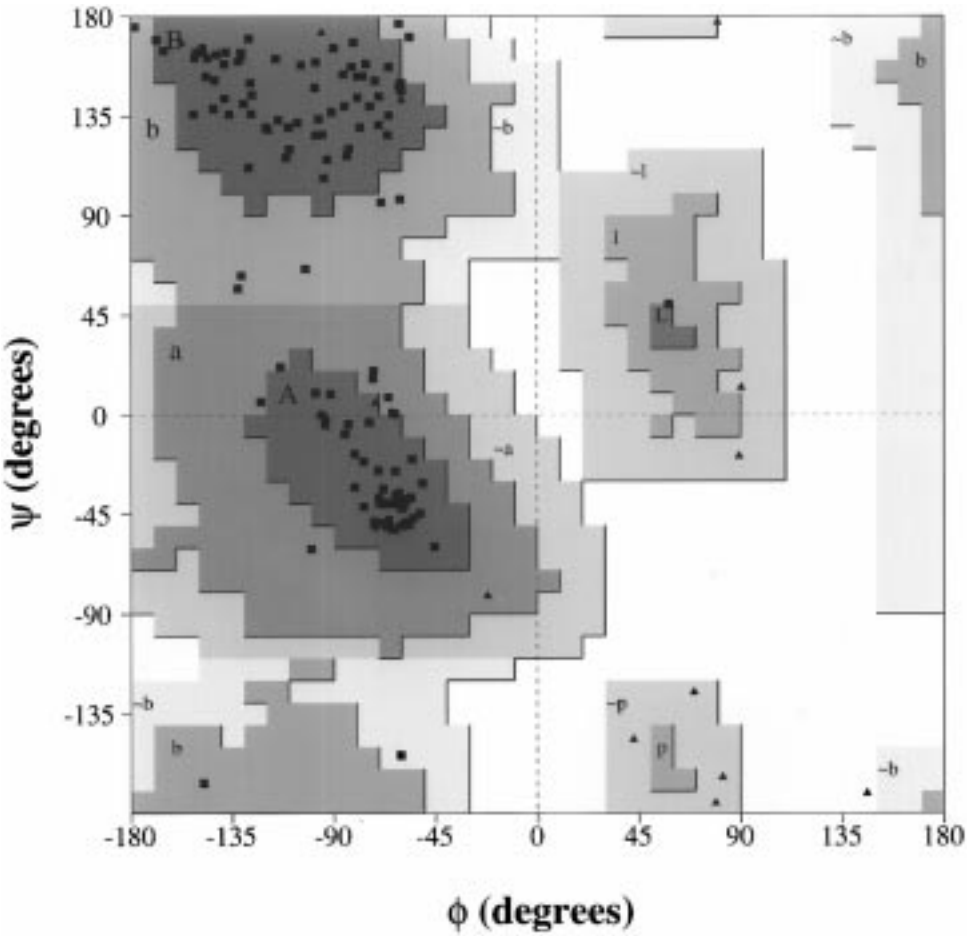

FIGURE 3: Ramachandran ϕ, ψ plot for the restrained minimized mean structure of MMP-1. The glycine residues are plotted as solid triangles.

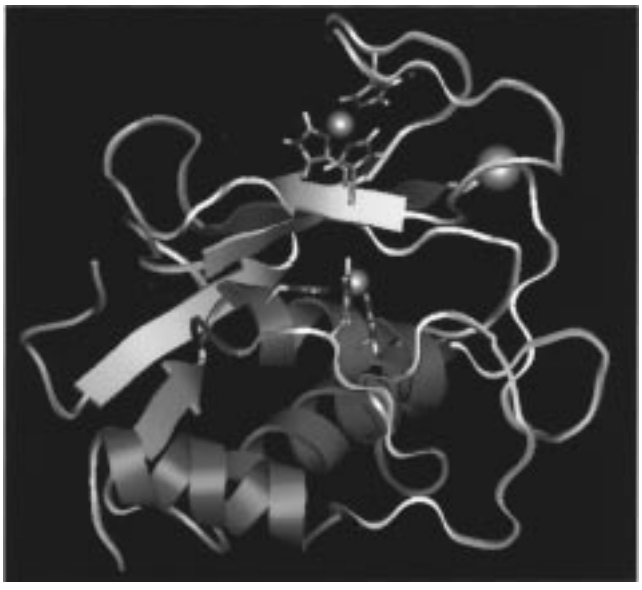

FIGURE 4: Ribbon drawing of the restrained minimized mean structure of MMP-1. The five β-strands are shown in yellow, the three helices are shown in purple, the calcium and zinc ions are shown as van der Waal spheres and the side-chains of the chelating histidines are shown. The model was generated with Quanta 4.1 (Molecular Simulations, Inc., San Diego).

residues play a crucial role in forming an extensive hydrogen-bonding network with peptide-like inhibitors (*1*, *19*, *21*, *60*). It is also apparent from the GRASP figure that the side chain of N80 occupies the active site and partially blocks access to the S1′ pocket in the free form of the enzyme.

A common feature of the matrix metalloproteinase family of enzymes is a high sequence homology between members of this family particularly in the active site region (*21*) which is consistent with the observed broad, overlapping substrate specificity (*2*, *11*). Thus, the MMP family is readily amenable to homology modeling based on the NMR structure of free MMP-1 presented here. Interestingly, there are a few distinct sequence differences between the MMPs in the active site region resulting in some subtle but significant effects on the characteristics of the MMP binding site. These differences may lead to inhibitor specificity between the MMPs, primarily by effecting the depth of the S1′ pocket and the electrostatic surface of the active site. For example, the arginine that caps the bottom of the S1′ pocket in MMP-1 is replaced by a leucine in a number of other MMPs.

A reaction mechanism for the cleavage of peptides by thermolysin has been previously proposed by Matthews et al. (*64*) and extended to the MMP-1 structure by Lovejoy et al. (*65*). A key feature of this mechanism is the coordination of a water molecule by E119 and the catalytic zinc near the carbonyl of the scissile bond. The coordinated water attacks the carbonyl of the scissile and donates a hydrogen to E119 to initiate cleavage of the peptide. An abundance of water molecules have been observed in the active site of MMP-1 in various X-ray structures (*1*, *19*, *21*, *60*) consistent with this mechanism. We explored the possibility of tightly bound water molecules in the active site cleft of MMP-1 by

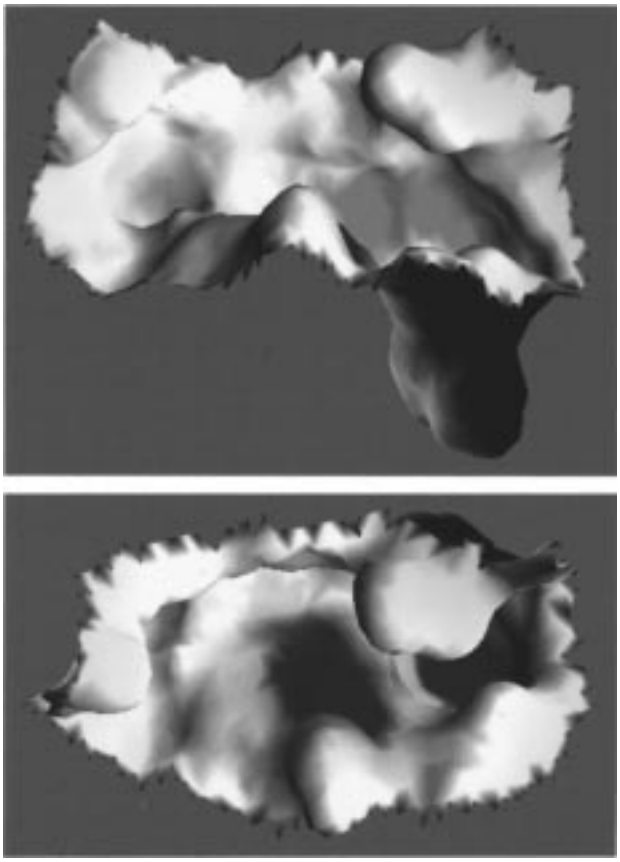

FIGURE 5: Two views of the electrostatic surface of the restrained minimized mean structure of MMP-1 corresponding to the active site region generated using the program GRASP (*66*). Blue and red indicate positively charged and negatively charged surfaces, respectively.

collecting a 3D ^{15}N-edited ROESY spectrum to determined if ROEs between water and backbone NHs could be observed in the active site region (data not shown).

While a number of ROEs to water were observed, the data indicated that no bound waters were detected in the vicinity of E119 or in the active cleft of MMP-1. The lack of an observed ROE to water in the vicinity of the catalytic zinc does not contradict the proposed mechanism of peptide cleavage by MMP-1 because of limitations in the experiment. It is plausible that a water molecule is bound to the catalytic zinc but that an ROE is not observed because it is not in close proximity to a backbone NH or it may have a lifetime shorter than 3×10^{-10} s (*61*). Since a water molecule in the vicinity of E119 and the catalytic zinc has only been seen in X-ray structures of MMPs containing an inhibitor, it is also plausible that the tight binding of the water molecule only occurs during or after substrate binding. Therefore, the appropriated interpretation of the negative NMR result is a lack of supportive evidence for the mechanism of MMP-1-mediated peptide cleavage without providing definitive evidence to contradict this hypothesis. The ROE data does suggest the presence of several bound water molecules to the protein surface usually adjacent to a group of Asp/Glu side chains.

Comparison of the Solution Structure of MMP-1 with the X-ray Structure. A number of refined X-ray structures for MMP-1 complexed to a variety of inhibitors have been previously determined (*1, 19, 21, 60*). In this paper, the high-resolution NMR solution structure of MMP-1 has been compared to the 1.56 Å X-ray structure of MMP-1 by Spurlino et al. (*1*) where MMP-1 is complexed to a hydroxamate inhibitor. The superposition of the backbone atoms of the restrained minimized, $(SA)_r$, NMR structure of MMP-1 with the X-ray structure is shown in Figure 6 with a plot of the backbone rms difference as a function of residue. Clearly, the overall fold of the two structures is similar, but distinct differences exists between the two structures, particularly in the active site region, as evident by the rms difference between the two structures. For residues 7−137 and 145−163, the atomic rms difference between the minimized mean NMR structure,(SA)r, and the X-ray structure is 1.22 Å for the backbone atoms and 1.69 Å for all atoms (Table 1). When only residues involved in secondary structure are considered, these values drop to 0.97 and 1.39 Å, respectively. The majority of the differences between the two structures appear to be in the active-site region; particularly the Ca^{2+} binding loop (residues 74−80) is "pushed-up" relative to the MMP-1 X-ray structure. Interestingly, a similar result was seen in the X-ray structure of MMP-1 complexed to itself (*21*).

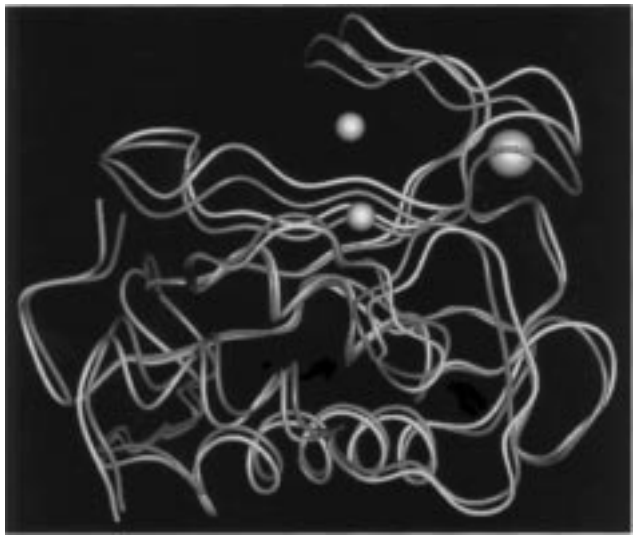

FIGURE 6: Best fit superposition of the backbone (N, Cα, and C) atoms of the restrained minimized mean NMR (blue) structure and the X-ray (yellow) structure of MMP-1 for residues 7−163 (A). Backbone (N, Cα, C, and O) atomic rms differences between the 30 simulated annealing structures and the X-ray structure as a function of residue number (B). The circles represent the average value at each residue and the error bars indicate the standard deviation of these values. The X-ray structure is that of Spurlino et al. (1994) (*1*).

It is important to note that the quality of the refinement of the Ca^{2+} binding loop was directly dependent on the presence of the calcium ion. Only sequential or short-range NOEs were observed for these residues, and since the loop also contains three glycines, identifying the proper dihedral restraints was problematic. The backbone dihedral restraints were identified by using a qualitative estimate of the magnitude of $^3J_{NH\alpha}$ coupling constants and from approximate distance restraints for intraresidue and sequential NOEs involving NH and CαH protons by means of the conformational grid search program STEREOSEARCH (*46*), but because of the large backbone conformational space available to glycine residues in the Ramachandran plot, a number of equivalent ϕ, ψ pairs were possible for the three glycines.

Table 2: Number of Violations Exhibited by the X-ray Structure of MMP-1 with Respect to the Experimental NMR Interproton Distance and Torsion Angle Restraints[a]

	A. Number of Violations in Interproton Distance Restraints					
	0.1−0.3 Å	0.3−0.5 Å	0.5−1.0 Å	1.0−2.0 Å	2.0−5.0 Å	>5.0 Å
all (2431)	25	16	16	5	2	0
interresidue sequential ($\|i-j\| = i$) (680)	8	3	3	2	1	0
interresidue short range ($1 < \|i-j\| \leq 5$) (482)	3	2	4	3	0	0
interresidue long-range ($\|i-j\| > 5$) (656)	4	5	3	0	1	0
intraresidue (529)	4	4	4	0	0	0
H-bonds (84)	6	2	2	0	0	0

	B. Violations in Torsion Angle Restraints			
	10−30°	30−60°	60−120°	>120°
all (407)	5	1	12	1
ϕ (146)	1	0	0	1
ψ (130)	3	1	1	0
χ_1 (97)	1	0	11	0
χ_2 (34)	0	0	0	0

[a] The X-ray structure of MMP-1 is the 1.56 Å resolution X-ray structure of Stams et al. (*15*). Residues 1−6 and 164−169 are not present in the X-ray structure. The total number of interproton distance and torsion angle restraints in each category is given in parentheses. Tyr and Phe χ_2 dihedral angles in the X-ray structure were changed to be consistent with the NMR structure since it is not possible to differentiate between +90° or −90° in the X-ray structure. Without this correction, the number of violations would be artificially high for the X-ray structure.

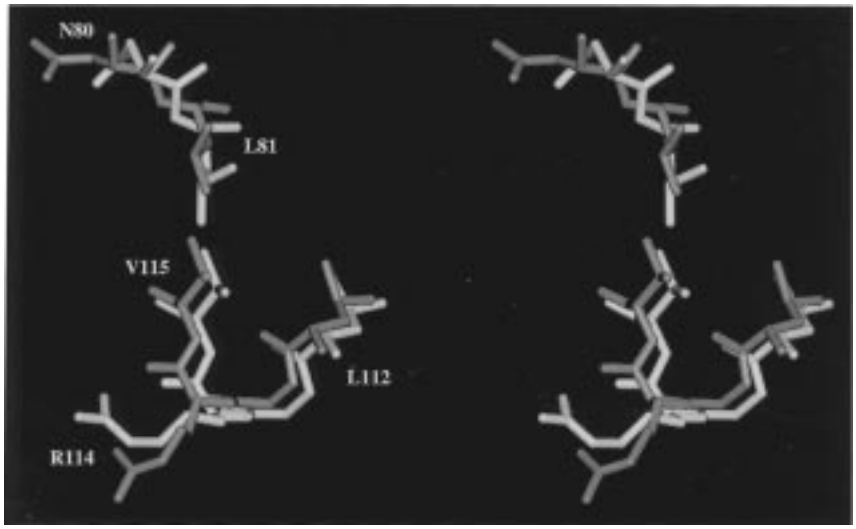

FIGURE 7: Best fit superposition of the backbone (N, Cα, and C) and side-chain heavy atoms of the restrained minimized mean NMR (blue) and the X-ray (yellow) structure of MMP-1 for residues N80, L81, L112, R114, and V115 which play a critical role in the MMP-1 active site.

Typically, the correct dihedral restraints are readily identified when the structure refinements converge to one predominate conformer, usually resulting from packing and long-range interactions. This did not occur in this case since the loop was solvent exposed and made no significant long-range interactions. Therefore, the structural data suggested that this loop was mobile and sampled a number of possible conformations. This was not consistent with the NMR dynamic data, since the order parameters ($S^2 > 0.8$) indicated that this loop region was well-defined. After incorporating the Ca^{2+} ion into the refinement protocol, this loop region became well-defined, and unique dihedral conformations for the glycines were identified. These results suggest that chelation of the Ca^{2+} ion by residues 74−80 is essential for establishing the proper local structure, and since these residues are in the vicinity of the active site, it would also suggest that proper chelation of Ca^{2+} is crucial for enzyme activity.

Another distinction between the NMR and X-ray structure of MMP-1 is the apparent mobility of residues 138−144. In a previous paper, we reported a dynamics study of inhibitor-free MMP-1 where the order parameters (S^2) for this loop region were <0.6 (*13*). This is consistent with the structure refinement of MMP-1 where residues 138−144 had a minimal number of NOEs resulting in a poorly defined structure relative to the remainder of the protein. While these residues exhibited a significant amount of disorder, the level of disorder may appear less than expected when compared to the disordered N- and C-terminus. This results from the nature of the protein structure in the vicinity of this disordered loop. Basically, the well-defined residues which flank the disordered loop are separated by ∼18 Å causing the intervening disordered loop to adopt an extended structure which significantly limits the available conformational space. In essence the residues are mobile while having a limited range of accessible conformations. This contrasts with the X-ray structures of MMP-1 complexed to an inhibitor where this portion of the protein is well-defined as apparent by low *B*-factors.

The local differences between the NMR and X-ray structures are indicated by the very high values of the NOE and torsion angle restraint energies (Table 1) and by the

number of interproton distance and torsion angle violations greater than 2 Å and 60°, respectively, exhibited by the X-ray structure (Table II). A significant number of the larger violations can be attributed to different χ rotamers. There are a total of 12 residues between the NMR and X-ray structures that have distinctly different χ_1. Of particular note is the χ_1 for N80 which is −179° in the X-ray structure compared to −60° in the NMR structure. This results in the side chain of N80 fitting into the active site of the NMR structure and partially blocking access to the S1′ pocket (Figure 5), whereas in the X-ray structure, N80 is in position to form potential hydrogen bond interactions with the inhibitor. This difference in the χ_1 for N80 was also seen in the X-ray structure of MMP-1 complexed to itself (*21*). A comparison between the NMR and X-ray structures for the residues which play a critical role in the active site of MMP-1 are shown in Figure 7. While the NMR rotamer constraints for the remainder of the critical active site residues are consistent with the X-ray structure, it is also apparent that differences still exist between the two structures. The remainder of the rotamer differences between the NMR and X-ray structure are for surface exposed residues where a change in side-chain conformation would not have a major impact on the overall protein structure.

There was also one significant backbone difference observed between the NMR and X-ray structure. In the X-ray structures, a cis-peptide bond was found for E109−Y110. There was no compelling evidence in the NMR data to identify a cis-peptide bond for this amino acid pair since the CαH proton chemical shifts were nearly degenerate. There was no difficulty in refining the NMR structure with a trans-peptide bond for E109−Y110, but as evident by the rms plot (Figure 2), this region of the protein had a relatively higher level of disorder which might account for the cis-peptide bond in the X-ray structure.

The studies described herein present the first high-resolution structural information for a matrix metalloproteinase in the absence of an inhibitor. The high-resolution NMR data clearly indicates a number of significant differences between the structure of MMP-1 in the presence and absence of an inhibitor. Not surprisingly, the majority of these differences occur in the vicinity of the active cleft and provide insight into the structural effect an inhibitor has on MMP-1 upon binding. Additionally, access to a inhibitor-free structure of MMP-1 provides an essential foundation for establishing a structure-based approach to designing inhibitors for MMP-1. Finally, because of the high-sequence homology between the MMPs, the NMR structure of inhibitor-free MMP-1 is ideally suited for developing homology models for other MMP proteins and for designing selective inhibitors.

REFERENCES

1. Spurlino, J. C., Smallwood, A. M., Carlton, D. D., Banks, T. M., Vavra, K. J., Johnson, J. S., Cook, E. R., Falvo, J., and Wahl, R. C., et al. (1994) *Proteins: Struct., Funct., Genet. 19*, 98−109.
2. Woessner, J. F., Jr. (1991) *Faseb J. 5*, 2145−54.
3. Ries, C., and Petrides, E. (1995) *Biol. Chem. Hoppe-Seyler 376*, 345−55.
4. Morphy, J. R., Millican, T. A., and Porter, J. R. (1995) *Curr. Med. Chem. 2*, 743−62.
5. Goldberg, G. I., Wilhelm, S. M., Kronberger, A., Bauer, E. A., Grant, G. A., and Eisen, A. Z. (1986) *J. Biol. Chem. 261*, 6600−5.
6. Muller, D., Quantin, B., Gesnel, M.-C., Millon-Collard, R., Abecassis, J., and Breathnach, R. (1988) *Biochem. J. 253*, 187−92.
7. Lowry, C. L., McGeehan, G., and LeVine, H. I. (1992) *Proteins: Struct., Funct., Genet. 12*, 42−48.
8. Feng, R., Castelhano, A. L., Billedeau, R., and Yuan, Z. (1995) *J. Am. Soc. Mass Spectrom. 6*, 1105−11.
9. Springman, E. B., Nagase, H., Birkedal-Hansen, H., and Van Wart, H. E. (1995) *Biochemistry 34*, 15713−20.
10. Grymes, R. A., Kronberger, A., and Bauer, E. A. (1993) *Clin. Dermatol. 9*, 69−85.
11. Birkedal-Hansen, H., Moore, W. G. I., Bodden, M. K., Windsor, L. J., Birkedal-Hansen, B., DeCarlo, A., and Engler, J. A. (1993) *Crit. Rev. Oral Biol. Med. 4*, 197.
12. Rockwell, A., Melden, M., Copeland, R. A., Hardman, K., Decicco, C. P., and DeGrado, W. F. (1996) *J. Am. Chem. Soc. 118*, 10337−8.
13. Moy, F. J., Pisano, M. R., Chanda, P. K., Urbano, C., Killar, L. M., Sung, M.-L., and Powers, R. (1997) *J. Biomol. NMR 10*, 9−19.
14. Bode, W., Reinemer, P., Huber, R., Kleine, T., Schnierer, S., and Tschesche, H. (1994) *EMBO J. 13*, 1263−9.
15. Stams, T., Spurlino, J. C., Smith, D. L., Wahl, R. C., Ho, T. F., Qoronfleh, M. W., Banks, T. M., and Rubin, B. (1994) *Nat. Struct. Biol. 1*, 119−23.
16. Botos, I., Scapozza, L., Zhang, D., Liotta, L. A., and Meyer, E. F. (1996) *Proc. Natl. Acad. Sci. U.S.A. 93*, 2749−54.
17. Broutin, I., Arnoux, B., Riche, C., Lecroisey, A., Keil, B., Pascard, C., and Ducruix, A. (1996) *Acta Crystallogr., Sect. D D52*, 380−92.
18. Gooley, P. R., O'Connell, J. F., Marcy, A. I., Cuca, G. C., Axel, M. G., Caldwell, C. G., Hagmann, W. K., and Becker, J. W. (1996) *J. Biomol. NMR 7*, 8−28.
19. Lovejoy, B., Cleasby, A., Hassell, A. M., Longley, K., Luther, M., A., Weigl, D., McGeehan, G., McElroy, A. B., Drewry, D., Lambert, M. H., and Jordan, S. R. (1994) *Science 263*, 375−77.
20. Van Doren, S. R., Kurochkin, A. V., Hu, W., Ye, Q.-Z., Johnson, L. L., Hupe, D. J., and Zuiderweg, E. R. P. (1995) *Protein Sci. 4*, 2487−98.
21. Lovejoy, B., Hassell, A. M., and Luther, M. A. (1994) *Biochemistry 33*, 8207−17.
22. Piotto, M., Saudek, V., and Sklenar, V. (1992) *J. Biomol. NMR 2*, 661−5.
23. Grzesiek, S., and Bax, A. (1993) *J. Am. Chem. Soc 115*, 12593−4.
24. Marion, D., Ikura, M., Tschudin, R., and Bax, A. (1989) *J. Magn. Reson. 85*, 393−9.
25. Vuister, G. W., and Bax, A. (1993) *J. Am. Chem. Soc. 115*, 7772−7.
26. Archer, S. J., Ikura, M., Torchia, D. A., and Bax, A. (1991) *J. Magn. Reson. 95*, 636−41.
27. Bax, A., and Pochapsky, S. S. (1992) *J. Magn. Reson. 99*, 638−43.
28. Powers, R., Gronenborn, A. M., Clore, G. M., and Bax, A. (1991) *J. Magn. Reson. 94*, 209−13.
29. Vuister, G. W., Delaglio, F., and Bax, A. (1992) *J. Am. Chem. Soc 114*, 9674−5.
30. Grzesiek, S., Kuboniwa, H., Hinck, A. P., and Bax, A. (1995) *J. Am. Chem. Soc 117*, 5312−15.
31. Marion, D., Driscoll, P. C., Kay, L. E., Wingfield, P. T., Bax, A., Gronenborn, A. M., and Clore, G. M. (1989) *Biochemistry 28*, 6150−6.
32. Zuiderweg, E. R. P., and Fesik, S. W. (1989) *Biochemistry 28*, 2387−91.
33. Zuiderweg, E. R. P., McIntosh, L. P., Dahlquist, F. W., and Fesik, S. W. (1990) *J. Magn. Reson 86*, 210−16.
34. Ikura, M., Kay, L. E., Tschudin, R., and Bax, A. (1990) *J. Magn. Reson 86*, 204−9.
35. Clore, G. M., Bax, A., Wingfield, P. T., and Gronenborn, A. M. (1990) *Biochemistry 29*, 5671−6.

36. Moy, F. J., Seddon, A. P., Boehlen, P., and Powers, R. (1996) *Biochemistry 35*, 13552−61.
37. Delaglio, F., Grzesiek, S., Vuister, G. W., Zhu, G., Pfeifer, J., and Bax, A. (1995) *J. Biomol. NMR 6*, 277−93.
38. Garrett, D. S., Powers, R., Gronenborn, A. M., and Clore, G. M. (1991) *J. Magn. Reson. 95*, 214−20.
39. Zhu, G., and Bax, A. (1992) *J. Magn. Reson. 100*, 202−7.
40. Williamson, M. P., Havel, T. F., and Wuethrich, K. (1985) *J. Mol. Biol 182*, 295−315.
41. Clore, G. M., Nilges, M., Sukumaran, D. K., Bruenger, A. T., Karplus, M., and Gronenborn, A. M. (1986) *EMBO J. 5*, 2729−35.
42. Wuthrich, K., Billeter, M., and Braun, W. (1983) *J. Mol. Biol. 169*, 949−61.
43. Clore, G. M., Gronenborn, A. M., Nilges, M., and Ryan, C. A. (1987) *Biochemistry 26*, 8012−23.
44. Wagner, G., Braun, W., Havel, T. F., Schaumann, T., Go, N., and Wuethrich, K. (1987) *J. Mol. Biol. 196*, 611−39.
45. Powers, R., Garrett, D. S., March, C. J., Frieden, E. A., Gronenborn, A. M., and Clore, G. M. (1993) *Biochemistry 32*, 6744−62.
46. Nilges, M., Clore, G. M., and Gronenborn, A. M. (1990) *Biopolymers 29*, 813−22.
47. Kraulis, P. J., Clore, G. M., Nilges, M., Jones, T. A., Pettersson, G., Knowles, J., and Gronenborn, A. M. (1989) *Biochemistry 28*, 7241−57.
48. Bax, A., Max, D., and Zax, D. (1992) *J. Am. Chem. Soc. 114*, 6923−5.
49. Powers, R., Garrett, D. S., March, C. J., Frieden, E. A., Gronenborn, A. M., Clore, G. M., Vuister, G. W., Clore, G. M., Gronenborn, A. M., Powers, R., Garrett, D. S., Tschudin, R., and Bax, A. (1993) *Biochemistry 32*, 6744−62.
50. Zuiderweg, E. R. P., Boelens, R., and Kaptein, R. (1985) *Biopolymers 24*, 601−11.
51. Nilges, M., Gronenborn, A. M., Bruenger, A. T., and Clore, G. M. (1988) *Protein Eng. 2*, 27−38.
52. Clore, G. M., Appella, E., Yamada, M., Matsushima, K., and Gronenborn, A. M. (1990) *Biochemistry 29*, 1689−96.
53. Brunger, A. T. (1993) *X-PLOR Version 3.1 Manual*, Yale University, New Haven, CT.
54. Garrett, D. S., Kuszewski, J., Hancock, T. J., Lodi, P. J., Vuister, G. W., Gronenborn, A. M., and Clore, G. M. (1994) *J. Magn. Reson., Ser. B 104*, 99−103.
55. Kuszewski, J., Qin, J., Gronenborn, A. M., and Clore. (1995) *J. Magn. Reson., Ser. B 106*, 92−6.
56. Kuszewski, J., Gronenborn, A. M., and Clore, G. M. (1996) *Protein Sci. 5*, 1067−80.
57. Kuszewski, J., Gronenborn, A. M., and Clore, G. M. (1997) *J. Magn. Reson. 125*, 171−77.
58. Clore, G. M., and Gronenborn, A. M. (1991) *Science 252*, 1390−9.
59. Forman-Kay, J. D., Clore, G. M., Wingfield, P. T., and Gronenborn, A. M. (1991) *Biochemistry 30*, 2685−98.
60. Borkakoti, N., Winkler, F. K., Williams, D. H., D'Arcy, A., Broadhurst, M. J., Brown, P. A., Johnson, W. H., and Murray, E. J. (1994) *Nat. Struct. Biol. 1*, 106−10.
61. Otting, G., and Wuthrich, K. (1989) *J. Am. Chem. Soc. 111*, 1871−75.
62. Forman-Kay, J. D., Gronenborn, A. M., and Wingfield, P. T. (1991) *J. Mol. Biol 220*, 209−16.
63. Clore, G. M., and Gronenborn, A. M. (1992) *J. Mol. Biol 223*, 853−6.
64. Matthews, B. W. (1988) *Acc. Chem. Res. 21*, 333−40.
65. Lovejoy, B., Cleasby, A., Hassell, A. M., and Longley. (1994) *Science 263* (5145), 375−7.
66. Nicholls, A., Sharp, K., and Honig, B. (1991) *Proteins: Struct., Funct., Genet. 11*, 281 ff.
67. Brooks, B. R., Bruccoleri, R. E., Olafson, B. D., States, D. J., Swaminathan, S., and Karplus, M. (1983) *J. Comput. Chem. 4*, 187−217.

BI972181W